Ceramics International 50 (2024) 13500–13507

Contents lists available at ScienceDirect

Ceramics International

journal homepage: www.elsevier.com/locate/ceramint

Effect of cation occupancy on crystal structure and microwave dielectric characteristics of spinel-structured (1-x)Zn_2TiO_4-$xli_2MgTi_3O_8$ ceramics

Yajie Wang [a,b], Ziyi Zhang [a,b], Jie Li [a,b,*], Ying Tang [c], Liang Fang [a,b]

[a] Guangxi Universities Key Laboratory of Non-ferrous Metal Oxide Electronic Functional Materials and Devices, College of Material Science and Engineering, Guilin University of Technology, Guilin, 541004, China
[b] Collaborative Innovation Center for Exploration of Nonferrous Metal Deposits and Efficient Utilization of Resources, Guilin University of Technology, Guilin, Guangxi, 541004, China
[c] College of Physics and Electronic Information Engineering, Guilin University of Technology, Guilin, 541004, China

ARTICLE INFO

Handling Editor: Dr P. Vincenzini

Keywords:
1-x)Zn_2TiO_4-$xLi_2MgTi_3O_8$
Disordered
Ordered spinel structure
Microwave dielectric properties

ABSTRACT

Excellent spinel microwave dielectric ceramics (1-x)Zn_2TiO_4-$xLi_2MgTi_3O_8$ (ZTLMTx, x = 1/3 and 2/3) were prepared at relatively low densification temperatures of 1100 °C and 1080 °C, respectively. A disordered cubic phase with space group *Fd*-3*m* was formed at x = 1/3, whereas an ordered cubic phase with space group $P4_332$ was formed at x = 2/3. The ceramics at x = 1/3 and 2/3 exhibited promising microwave dielectric properties of ε_r = 18.27 and 22.96, $Q \times f$ = 91,877 GHz and 75,186 GHz, and τ_f = −42.3 ppm/°C and −21.05 ppm/°C, respectively. The large deviation between the experimental ε_r and theoretical ε_{th} of 1/3 and 2/3 ceramics were 18.3 % and 57 %, respectively, due to the underestimation of the ionic polarizability of Ti^{4+}. The difference in their ε_r, $Q \times f$, and τ_f were discussed by the structure, FWHM of A_{1g}, lattice energy and bond energy in detail.

1. Introduction

Microwave dielectric ceramics, as an important class of electronic ceramic materials, play a pivotal role in the field of modern wireless communications, such as satellite navigation, mobile communications, radar, and many other fields [1,2]. With the development of 5G communications technology to millimeter wave band, the working frequency of 24–30 GHz, or 60–70 GHz, the delay time of signal transmission (less than 1 ms) has been greatly reduced [3,4]. Therefore, in order to ensure the transmission of high-quality signals, the performance of microwave dielectric ceramics is increasingly demanding. A low dielectric constant (ε_r) helps to inhibit signal delay, a high quality factor ($Q \times f$) can enhance the signal strength, and an approaching-zero τ_f is conducive to the stable operation of the devices [5–8]. Microwave dielectric ceramics with excellent integrative performance are of great interest to researchers and commercial entities.

In recent years, spinel-structured ceramics have been gained considerable attention and exploration due to their outstanding physicochemical and good structural tunability [9–16]. Zn_2TiO_4, an inverse spinel with a space group of *Fd*-3*m*, is a promising candidate for microwave dielectric applications because of its favorable microwave dielectric performance (ε_r = 21, $Q \times f$ = 50,000 GHz, and τ_f = −60 ppm/°C) and relatively low sintering temperature (1100 °C) [17]. In particular, compared with Al, Ga-based and Mg_2TiO_4 [18] ceramics with the same crystal structure, Zn_2TiO_4 can be sintered densified at a temperature of 350–500 °C lower than them, which greatly reduces energy loss. In contract, the $Q \times f$ value of Zn_2TiO_4 is poor and the τ_f is large negative.

Researchers have tried to design a series of doping components, hoping to improve the microwave dielectric performance of Zn_2TiO_4, such as $(Zn_{1-x}Cu_x)_2TiO_4$ ($0 \le x \le 0.20$) and $(Zn_{0.95}M_{0.05})_2TiO_4$ (M = Mn^{2+}, Co^{2+}, Ni^{2+}, Cu^{2+}) ceramics [19,20]. But only $(Zn_{0.8}Cu_{0.2})_2TiO_4$ ceramic features an improved τ_f value (−15.4 ppm/°C) without $Q \times f$ optimizing. Besides, Shih et al. [21] acquired a near-zero τ_f by forming two-phase composite ceramics with rutile phase TiO_2, but resulted in an extremely poor $Q \times f$. Many studies concluded that the cation occupation and structural ordering distribution in spinels have important effects on their microwave dielectric properties. Zuo et al. [22] substituted the Zn^{2+} of $Zn_2TiO_4$with the $[Li_{2/3}Ti_{1/3}]^{2+}$ complex, and found that the $Q \times f$ of the system can be increased up to 160,000 GHz in the disordered phase (*Fd*-3*m*), and the minimum value of the τ_f (−20 ppm/°C) appears with the emergence of the ordered phase ($P4_332$). Similar results have

* Corresponding author. Guangxi universities key laboratory of non-ferrous metal oxide electronic functional materials and devices, College of Material Science and Engineering, Guilin University of Technology, Guilin, 541004, China.
E-mail address: jielee@glut.edu.cn (J. Li).

https://doi.org/10.1016/j.ceramint.2024.01.262
Received 7 November 2023; Received in revised form 5 January 2024; Accepted 19 January 2024
Available online 26 January 2024

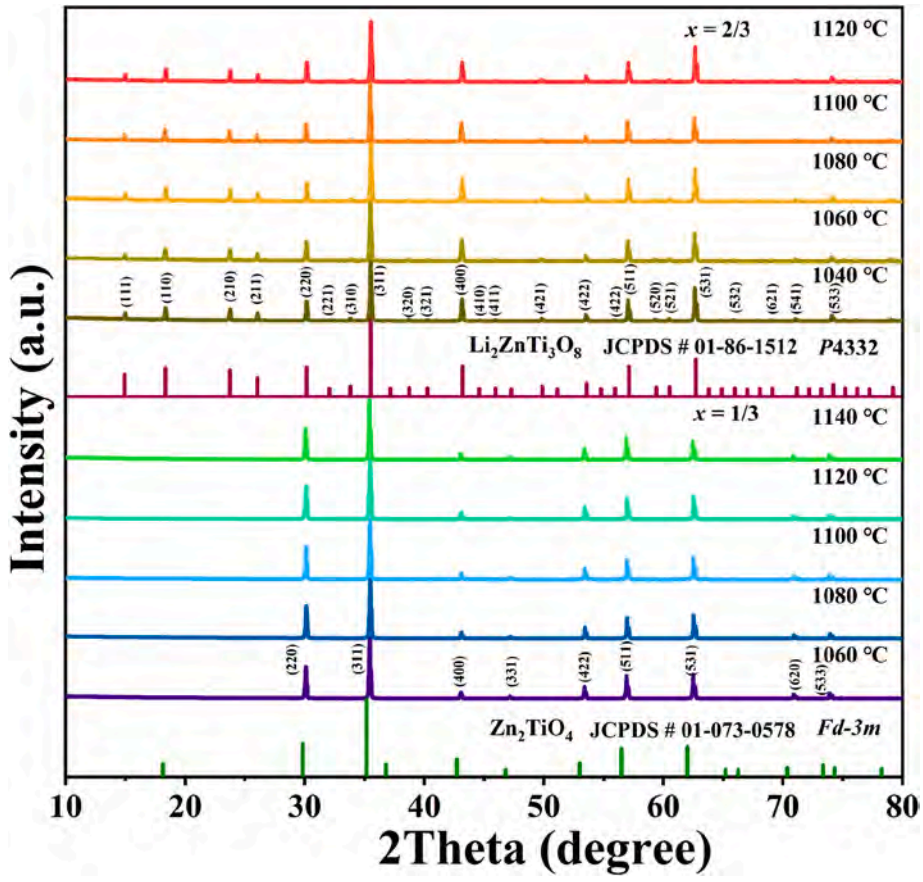

Fig. 1. XRD patterns of $x = 1/3$ and 2/3 ceramics.

been observed in our previous study of the $Zn_{2-2x}Li_xGa_{4+x}O_8$ ($0 \le x \le 1$) system [23], where the maximum of $Q \times f$ (120,370 GHz) is found in the disordered phase (*Fd*-3*m*), while the appearance of the ordered phase ($P4_332$) minimizes the τ_f. These results demonstrate that the change of composition leads to the difference in the structure, which has a significant effect on the $Q \times f$ and τ_f of microwave dielectric ceramics. The B-site 1:3 ordered $Li_2MTi_3O_8$ (M = Zn, Mg) [24] are valued for their near-zero τ_f and good $Q \times f$, which has attracted many researchers to study their modification [25,26]. $Li_2MgTi_3O_8$ ceramic with $P4_332$ space group exhibits a rarely close-zero τ_f value of +3.2 ppm/°C, along with ε_r = 27.2, $Q \times f$ = 42,000 GHz and low densification temperature of 1075 °C [27]. Therefore, we consider that the introduction of $Li_2MgTi_3O_8$ into Zn_2TiO_4 ceramics to improve the microwave dielectric properties without increasing the sintering temperature.

In this study, we prepared ZTLMT*x* ceramics by the solid-state reaction method, and focused on the relationship between the crystal structure, phase composition and microwave dielectric properties. The crystal structures and cation ordering of the ceramics were analyzed using Rietveld refinement, Raman spectroscopy, and high-resolution transmission electron microscopy (TEM). Additionally, the relationship between lattice energy, bond energy, ionicity and intrinsic microwave dielectric properties was investigated based on the Phillips-Van Vechten-Levine (P–V–L) theory.

2. Experimental procedures

ZTLMT*x* (x = 1/3 and 2/3) ceramics were fabricated by the solid-state method with high-purity Li_2CO_3 (99.99 %, Aladdin), ZnO (99.99 %, Aladdin), MgO (99.99 %, Aladdin), and TiO_2 (99.99 %, Aladdin) as raw materials. Stoichiometrically weighed raw materials were mixed in a ball mill using anhydrous alcohol as a milling medium for 6 h. Then, the resultant slurry was dried and calcined at 900 °C for 4 h. Re-milled for 6h and dried, the dried powders mixed with 5 wt% PVA and pressed into cylindrical pellets (6 mm in height and 10 mm in diameter). Finally, the cylinders were calcined at 550 °C for 1 h to remove the PVA and then sintered at 1040–1140 °C for 6 h.

The X-ray diffraction analysis (XRD, Model X'Pert PRO) was performed to determine the crystal structures of ZTLMT*x* ceramics. The Rietveld refinement for XRD data was carried out using the FullProf program. After the ceramic powder was prepared into suspension, the crystal structure and ordering of the ceramics were further investigated by the JEOL JEM-2100 F TEM. The polished ceramic samples were thermally etched at a temperature of 50 °C below the optimum sintering temperature for half an hour, scanning electron microscopes (FESEM; S4800, Hitachi, Tokyo, Japan) was used to conduct microstructure analysis. The grain sizes were determined using the linear intercept method [28]. Room temperature Raman spectra were collected using a Raman spectrometer equipped with a 532 nm laser (DXR, Thermo Fisher Scientific). The microwave dielectric properties of the samples were evaluated using a network analyzer (N5230A, Agilent). The τ_f was obtained using a temperature chamber (Delta 9039, Delta Design, San Diego, CA), and calculated as our previous works [29,30].

3. Results and discussions

Fig. 1 presents the XRD patterns of $x = 1/3$ and 2/3 ceramics sintered at various temperatures from 1040 °C to 1140 °C. All the diffraction peaks of $x = 1/3$ ceramic could be well indexed with the standard card (JCPDS # 01-073-0578) of disordered spinel Zn_2TiO_4 phase. However, the diffraction peaks of $x = 2/3$ ceramic are perfectly matched with the standard card (JCPDS # 01-086-1512) of ordered spinel $Li_2ZnTi_3O_8$. No secondary phase is detected in both ceramics. It can be inferred that x =

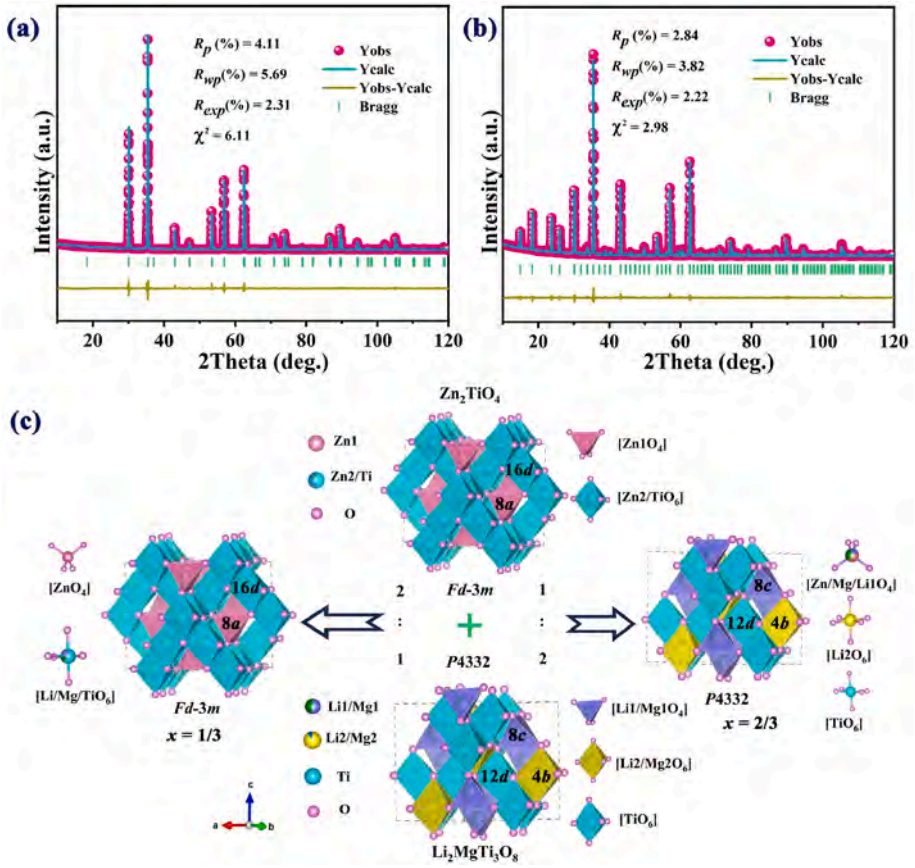

Fig. 2. (a)–(b) Rietveld refinement results of XRD data for x = 1/3 and 2/3 ceramics sintered at 1100 °C and 1080 °C, respectively; (c) Formation schematic representation and cation distribution of both ceramics.

Table 1
Atomic occupation information of x = 1/3 and 2/3 ceramics.

Ceramics	Atoms	x	y	z	Occupy	Wyckoff position
x = 1/3	Zn	0.12500	0.12500	0.12500	1	8*a*
	Mg	0.50000	0.50000	0.50000	0.125	16*d*
	Ti1	0.50000	0.50000	0.50000	0.625	16*d*
	Li	0.26110	0.26110	0.26110	0.25	16*d*
	O1	0.26157	0.26157	0.26157	1	32*e*
x = 2/3	Zn	−0.00100	−0.00100	−0.00100	0.4	8*c*
	Mg	−0.00100	−0.00100	−0.00100	0.4	8*c*
	Li1	−0.00100	−0.00100	−0.00100	0.2	8*c*
	Li2	0.62500	0.62500	0.62500	1	4*b*
	Ti	0.36264	0.87719	0.11971	1	12*d*
	O1	0.11019	0.11019	0.38640	1	24*e*
	O2	0.38844	0.38844	0.38844	1	8*c*

1/3 ceramic exhibits a face-centered cubic disordered spinel structure with space group *Fd*-3*m*, while x = 2/3 ceramic is a primitive cubic ordered spinel with space group $P4_332$.

Detailed component-structure information of both ceramics was investigated by Rietveld refinement of the slow-scanning XRD data. The Rietveld refinement of x = 1/3 and 2/3 ceramics sintered at 1100 °C and 1080 °C, respectively, are shown in Fig. 2(a–b), and the results for the other sintering temperatures are presented in Figs. S1 and S2 (Supporting Information). Low-reliability factors (R_{wp}, R_{exp}, R_p and χ^2) indicate close correspondence between the observed and the calculated patterns. The refinement results indicate that the x = 1/3 ceramic can be indexed as a disordered spinel (*Fd*-3*m*), while the ceramic at x = 2/3 exhibits an ordered spinel structure ($P4_332$). The refined cell volume (V) of x = 1/3 and 2/3 are 593.74 Å^3 and 590.72 Å^3, respectively. The larger V for 1/3 than 2/3 originates from the fact that the V of Zn_2TiO_4 (607.236 Å^3) is larger than that of $Li_2MgTi_3O_8$ (591.430 Å^3) [19,24].

The schematic diagrams of the formation of different structures of Zn_2TiO_4–$Li_2MgTi_3O_8$ system are clearly depicted in Fig. 2(c), and the corresponding cation occupancy information is presented in Table 1. Since the Zn^{2+} cations preferentially occupy tetrahedral sites [16,31,32], all Zn^{2+} cations monopolize the A-site (8*a*) for x = 1/3 ceramic, the remaining Li^+, Mg^{2+}, and Ti^{4+} cations together occupy the octahedral sites (16*d*), forming a disordered structure with a space group *Fd*-3*m*. For x = 2/3 ceramic, DFT calculations show that the site where Mg^{2+} replaces Zn^{2+} has the lowest formation energy of −168.62 eV [33], and the two have similar ionic radii (R_{Zn2+} = 0.6 Å, R_{Mg2+} = 0.57 Å, CN = 4). Therefore, both Zn^{2+} and Mg^{2+} occupy the tetrahedral position 8*c*, and the remaining tetrahedral centers are filled by Li^+. Li^+ and Ti^{4+} occupy 4*b* and 12*d* sites, respectively, forming an ordered arrangement structure.

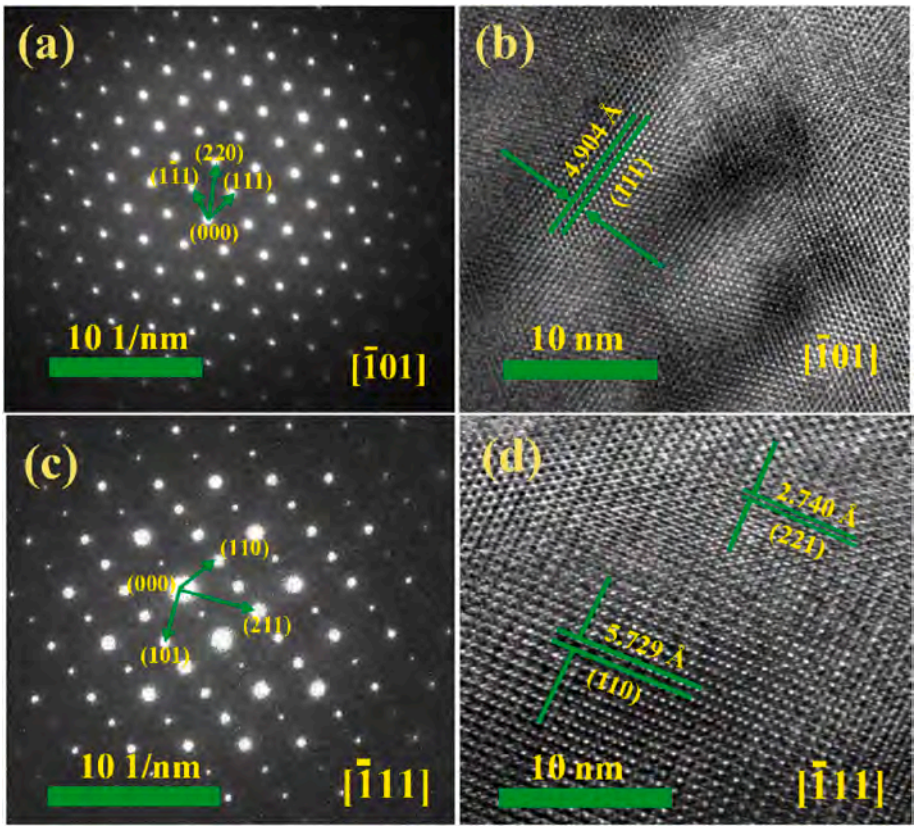

Fig. 3. SAED and HRTEM images of $x = 1/3$ and 2/3 ceramics taken along the [01] and [11] zone axes at room temperature, respectively.

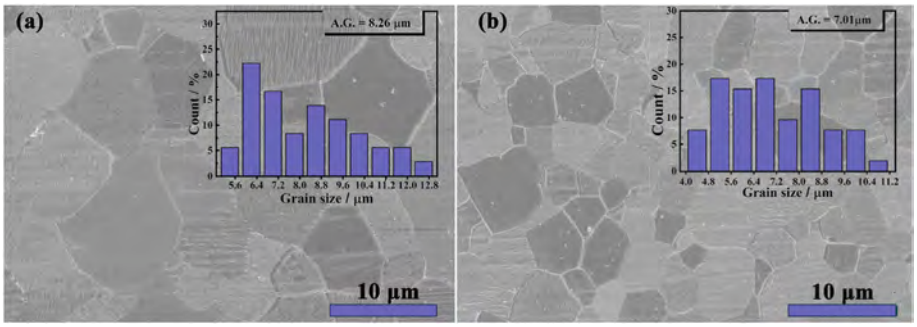

Fig. 4. SEM images of $x = 1/3$ and 2/3 ceramics sintered at (a) 1100 °C and (b) 1080 °C, and the distribution details of grains.

SAED and HRTEM were used to further study the ordered-disordered structure of $x = 1/3$ and 2/3 ceramics (see in Fig. 3). The SAED patterns consists of sharp diffraction spots, indicating that both the $x = 1/3$ and 2/3 grains have good crystallinity. The crystallographic planes (111) and (220) have been identified in $x = 1/3$ ceramic, and the crystallographic spacing of close-packed plane (111) is calculated to be 4.904 Å (Fig. 3(a-b)), suggesting the formation of a face-centered cubic disordered structure similar with that of Zn_2TiO_4. However, the superlattice diffraction planes (110) and (211) are observed in ceramics at $x = 2/3$, as shown Fig. 3 (c) and (d). The plane (110) corresponding to a crystallographic spacing of 5.729 Å indicates the formation of a primitive cubic ordered phase structure. The above results agree with the XRD analysis.

Fig. 4 shows the SEM images of the microstructure of $x = 1/3$ and 2/3 ceramics sintered at optimal temperatures, along with the distribution of grain size. Dense and uniform microstructures with almost no pores and well-defined grain boundaries were observed in both $x = 1/3$ and 2/3 ceramics. The grain size of ceramic at $x = 1/3$ (average grain ~8.26 μm) is significantly larger than that of ceramic at $x = 2/3$ (average grain ~7.01 μm). This may be due to the packing of ordered phases, which produces a certain inhibition of the grain growth [34].

The bulk densities of $x = 1/3$ and 2/3 ceramics sintered at their densification temperatures were obtained using the Archimedes drainage method as 4.32 g/cm^3 and 3.8 g/cm^3. Their theoretical densities were refined as 4.45 g/cm^3 and 3.88 g/cm^3, respectively. This difference may be primarily attributed to the distinct crystal structures of the two ceramics. Fig. 5(a) illustrates the relative density of the two ceramics as a function of sintering temperatures. The relative density of $x = 1/3$ and 2/3 ceramics first increased and then reached a saturation point of 97.0 % and 97.8 % at 1100 °C and 1080 °C, respectively. Subsequently, the relative density gradually declined with temperature continuing to rise. Besides, it is noteworthy that the relative density of both ceramics remained above 95 % at all sintering temperatures, indicating that the impact of porosity on their microwave dielectric properties is minimal.

Fig. 5(b–d) exhibit the microwave dielectric properties of $x = 1/3$

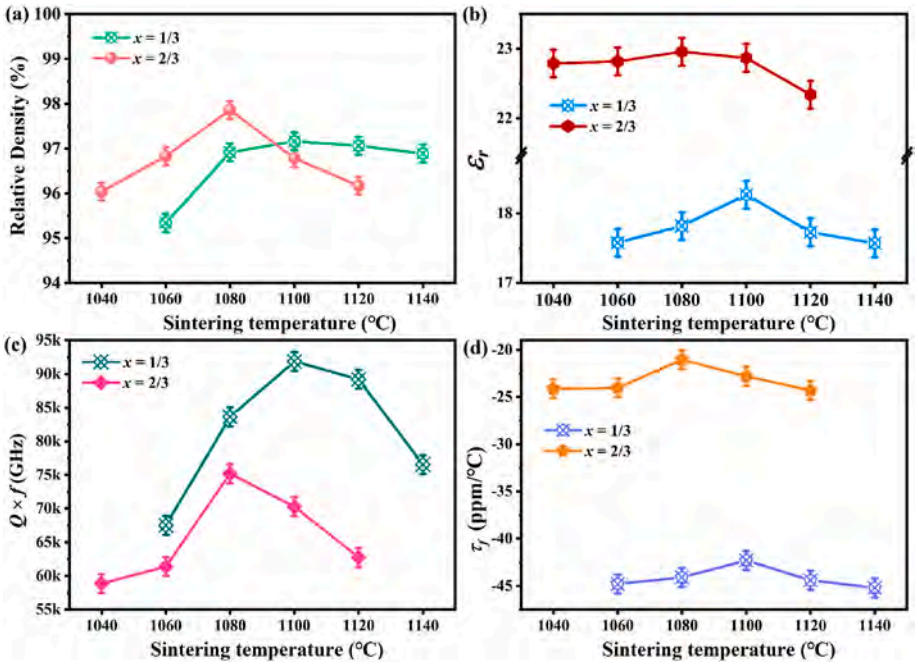

Fig. 5. (a) Relative density, (b) dielectric constant, (c) $Q \times f$, (d) τ_f values of the $x = 1/3$ and 2/3 ceramics sintered at various temperatures.

Table 2
ρ, ε_r, ε_{th}, V and ionic polarizability of several Ti-based spinel ceramics.

Ceramics	ρ (%)	ε_r	ε_{th}	Δ (%)	V (Å^3)	α_{Ti4+} (Å^3)	Δ_{Ti4+}	Ref
Zn_2TiO_4	94.7	19.8	15.7	26	607.236	3.51	20 %	[19]
Mg_2TiO_4	96	14.6	10.4	40	601.696	4.03	38 %	[18]
$LiZn_2Ti_2GaO_8$	96.3	17.1	14.5	18	588.288	3.37	15 %	[36]
$LiMg_2Ti_2GaO_8$	96.4	15.8	11.6	36	586.432	3.84	31 %	[36]
$Li_2ZnTi_3O_8$	96.2	25.6	16.1	59	591.430	3.96	35.2 %	[37]
$Li_2MgTi_3O_8$	95.5	27.2	13.7	98.5	588.698	3.60	22.9 %	[24]
$ZnMgTiO_4$	95.9	16.8	13.04	29	599.748	3.64	24	[38]
$x = 1/3$	97	18.27	15.45	18.3	593.752	3.27	11.6 %	This work
$x = 2/3$	97.8	22.97	14.62	57	590.723	3.68	25.6 %	

and 2/3 ceramics as a function of sintering temperature. With the increase in sintering temperature, the ε_r of $x = 1/3$ and 2/3 ceramics first increased to the maximum values of 18.27 and 22.96, and then slightly decreased. Their difference in ε_r may be mainly attributed to the high ionic polarizability of Ti^{4+} cation. In order to further investigate the effect of ionic polarizability on ε_r, the theoretical dielectric constants (ε_{th}) of ZTLMTx ($x = 1/3$ and 2/3) ceramics were calculated by the Clausius-Mosotti equation [35]:

$$\varepsilon_{th} = \frac{3V + 8\pi\alpha_T}{3V - 4\pi\alpha_T} \quad (1)$$

where V is the molecular volume, α_T is the molecular polarizability. Based on the Shannon's additive rule and crystal structure of ZTLMTx ceramics, $\alpha(x = 1/3) = \alpha(Zn^{2+}) + 0.5\alpha(Li^{+}) + 0.25\alpha(Mg^{2+}) + 1.25\alpha(Ti^{4+}) + 4\alpha(O^{2-})$, and $\alpha(x = 2/3) = 0.8\alpha(Zn^{2+}) + 0.8\alpha(Mg^{2+}) + 1.6\alpha(Li^{+}) + 2.8\alpha(Ti^{4+}) + 8\alpha(O^{2-})$. The ε_{th} values of $x = 1/3$ and 2/3 ceramics were calculated as 15.45 and 14.62, respectively, which were significantly lower than the experimental ε_r values (18.27 and 22.96), with relative deviation values (Δ (%) = $[(\varepsilon_r - \varepsilon_{th})/\varepsilon_{th}]$ *100 %) of 18.3 % and 57 %, respectively (See in Table 2). Fang et al. have reported that the underestimation of Shannon's ionic polarizability of Ti^{4+} results in the large deviations of 30.3 % for $LiMg_2GaTi_2O_8$ and 19.6 % for $LiZn_2GaTi_2O_8$ between the corrected ε_{corr} and theoretical ε_{th} [36]. Based on equation (1) and the oxide additivity rule, the experimental ionic polarizabilities of Ti^{4+} of $x = 1/3$ and 2/3 ceramics were calculated to be 3.27 and 3.68 Å^3, respectively, which were 11.6 % and 25.6 % higher than the Ti^{4+} ionic polarizability reported by Shannon (2.93 Å^3), as shown in Table 2.

Table 3
ε_r, ε_{corr}, E_{total} for $x = 1/3$ and 2/3 ceramics.

Ceramics	ε_r	ε_{corr}	E_{total} (kJ/mol)
$x = 1/3$	18.27	18.52	1436
$x = 2/3$	22.97	23.18	5947

As shown in Fig. 5(b), the slight change in ε_r of both ceramics with sintering temperature is similar to that of their relative density, which is closely related to the high relative density (>95 %) of the ceramics. The ε_r of both ceramics increase with the increase in sintering temperature [39]. Therefore, in order to assess the effect of porosity on ε_r, which was corrected with the following equation [40]:

$$\varepsilon_r = \varepsilon_{corr}\left(1 - \frac{3P(\varepsilon_{corr} - 1)}{2\varepsilon_{corr} + 1}\right) \quad (2)$$

where P represents the porosity fraction, and ε_{corr} and ε_r are the corrected and the measured ε_r, respectively. The corrected ε_{corr} were 18.52 for $x = 1/3$ and 23.18 for $x = 2/3$ (Table 3), indicating that the difference between ε_r and ε_{corr} was almost negligible, which was consistent with the relative density.

Fig. 5(c) demonstrates the variation of $Q \times f$ with sintering

Table 4
Microwave dielectric properties and sintering temperatures of spinel ceramics.

Ceramics	S.T. (°C)	ε_r	$Q \times f$ (GHz)	τ_f (ppm/°C)	References
$ZnAl_2O_4$	1600	8.5	106,000	−63	[9]
$MgAl_2O_4$	1600	8.75	68,900	−75	[10]
$ZnGa_2O_4$	1400	10.05	94,600	−71	[11]
$MgGa_2O_4$	1460	9.3	93,000	−64	[12]
Mg_2TiO_4	1450	14.51	150,000	−50	[18]
Zn_2TiO_4	1100	21	50,000	−60	[17]
$LiGa_5O_8$	1260	10.51	127,040	−60.2	[13]
$Li_2ZnTi_3O_8$	1075	25.6	72,000	−11.2	[24]
$Li_2MgTi_3O_8$	1075	27.2	42,000	+3	[24]
$x = 1/3$	1100	18.27	91,877	−42.3	This work
$x = 2/3$	1080	22.96	75,186	−21.3	

temperature. The $Q \times f$ values of the $x = 1/3$ and 2/3 ceramics first increase rapidly with increasing temperature, reaching the maximum values of 91,877 GHz and 75,186 GHz at the densification temperatures of 1100 °C and 1080 °C, respectively, and then descend rapidly. The subsequent decrease in $Q \times f$ is greatly dependent on the effect of sintering temperature on the relative density. The porosity and the secondary phase are not considered because of the high density and the results of the XRD. According to the report of Kim et al., increasing packing fraction will reduce the lattice vibration and thus enhance the $Q \times f$ value [41]. However, the packing fraction of the $x = 1/3$ and 2/3 ceramics are calculated to be 63.9 % and 64.0 %, respectively, which is inversely proportional to their $Q \times f$. It shows that there are other factors affecting the quality factor in these ceramics. Specific ordered structures can construct Li^+ transport channels that increase conductivity and conduction losses, thereby leading to a decrease in $Q \times f$ values [22,42]. For $x = 2/3$ ceramic, more Li^+ can migrate from the site 8*c* to the vacant octahedral site 4*b*, resulting in decreasing $Q \times f$.

Fig. 5(d) displays the temperature-dependent information of τ_f of $x = 1/3$ and 2/3 ceramics. The τ_f values of $x = 1/3$ and 2/3 ceramics fluctuate around −42.3 ppm/°C and −21.05 ppm/°C, respectively, with a weak dependence on sintering temperature. It is evident that the ceramic at $x = 2/3$ exhibits a closer to zero τ_f compared to that of $x = 1/3$. Some studies [43–45] have demonstrated that there is a strong dependence between bond energies (E_{total}) and τ_f. The E_{total} of the two ceramics are listed in Table 3. The ceramic at $x = 2/3$ has a higher bond energy (5947 kJ/mol) than ceramic at $x = 1/3$ (1436 kJ/mol), which is consistent with the correlation observed for τ_f.

A comparison (Table 4) has been drawn between the sintering temperatures and microwave dielectric properties of some spinel ceramics and ZTLMT*x* ($x = 1/3$ and 2/3) ceramics. $x = 1/3$ and 2/3 ceramics show much lower sintering temperatures and closer to zero τ_f than those of Al, Ga, and Ti-based ceramics. Meanwhile, the $Q \times f$ of $x = 1/3$ and 2/3 ceramics are higher than that of $Li_2ZnTi_3O_8$ and $Li_2MgTi_3O_8$ ceramics. Especially, The $Q \times f$ of $x = 1/3$ and 2/3 ceramics are increased by about 50 % compared with the end elements Zn_2TiO_4 and $Li_2MgTi_3O_8$.

Raman spectrum is an effective tool to study the lattice vibration information, whose variation causes changes in Raman shift and Raman full width at half maximum (FWHM). The Raman spectra and the Gaussian Lorentz modes of ZTLMT*x* ($x = 1/3$ and 2/3) ceramics are presented in Fig. 6(a). For the ceramic at $x = 1/3$, the peak at 393 cm^{-1} can be indexed as the A_{1g} mode of the ZnO_4 tetrahedron [22], which gives sufficient evidence that Zn^{2+} preferentially occupies the tetrahedral position, consistent with the XRD data results. The Raman modes at 739 and 821 cm^{-1} are attributed to the stretching vibrations of M−O bonds in the MO_6 octahedron. For the $x = 2/3$ ceramic, the A_{1g} and F_{2g} modes observed in the bands of 442–731 cm^{-1} are attributed to the stretching vibrations of the bonds in the MO_6 octahedra. Furthermore, the A_{1g} and F_{2g} vibrational modes in the 300–442 cm^{-1} are caused by the stretching vibrations of the Li/Zn/Mg–O bonds in the Li/Zn/MgO_4 tetrahedra. The bending vibrations of the O–Li/Zn/Mg/Ti–O bonds give rise to the E_g modes below 165-300 cm^{-1} [46]. As seen in Fig. 6(a), the A_{1g} peak around 400 cm^{-1} produces by the MO_6 octahedron of $x = 2/3$ ceramic is much sharper than that of $x = 1/3$, which is attributed to the ordered structure in the B-site of $x = 2/3$ ceramic. The variation in the FWHM of A_{1g} mode and $Q \times f$ values with increasing sintering temperature is illustrated in Fig. 6(b). In general, with the decrease in FWHM, the space of lattice vibration and the nonharmonic vibration decrease, thereby resulting in the decrease in inherent dielectric loss [47]. The FWHM of A_{1g} of $x = 1/3$ ceramic is narrower than that of $x = 2/3$ ceramic, corresponding to a higher $Q \times f$ of $x = 1/3$ ceramic than that of $x = 2/3$.

The P–V–L chemical bond theory [48,49] was used to calculate the ionicity (f_i^μ) and lattice energy (U_b^μ) of each chemical bond in ZTLMT*x* ($x = 1/3$ and 2/3) ceramics to deeply investigate the relationship between crystal structure and microwave dielectric properties. Detailed calculation process and results can be found in Table S2 (Supplementary Information). The analysis of the contribution of each bond to ε_r is depicted in Fig. 7(a). The Ti–O bonds contribute similarly (21.1 % and 20.8 %) to the ε_r of both ceramics, due to the both occupation of Ti^{4+} in octahedral sites. Additionally, the ε_r of $x = 2/3$ ceramic is higher than that of $x = 1/3$ ceramic, which is closely related to the increase in the total contribution (79.2 % for 2/3 and 78.9 % for 1/3, respectively) of Li–O, Mg–O and Ti–O bonds to ε_r. And the bonds in the octahedra of $x = 2/3$ ceramic have higher average-f_i^μ (0.8051) than those (0.7395) of $x = 1/3$ ceramics. Fig. 7(b) indicates that Ti^{4+} plays a crucial role in the U_b^μ of the ceramics. The average U_b^μ of the Ti–O bonds in the $x = 1/3$ (16, 641.45 kJ/mol) ceramics is much higher than that of the $x = 2/3$ (12, 224.34 kJ/mol), resulting in a higher $Q \times f$ of $x = 1/3$ ceramic than that of $x = 2/3$ ceramic. Besides, the total contribution of both Ti–O bonds and Zn–O bonds to U_b^μ decreases with increasing *x* shown in Fig. 7(c).

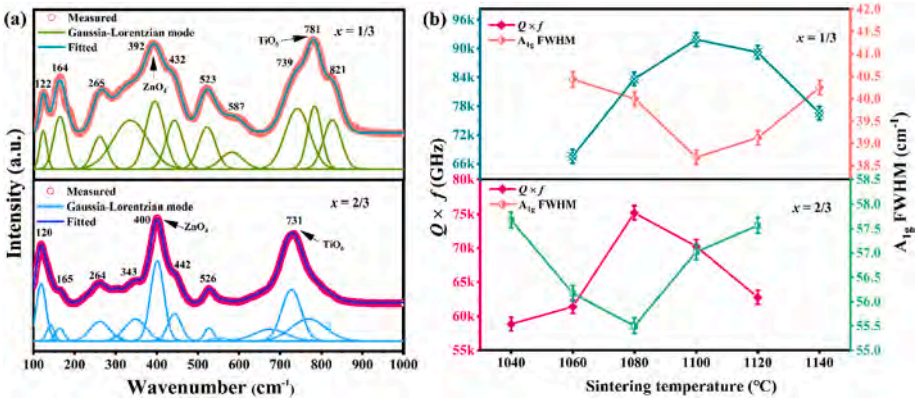

Fig. 6. (a) The room-temperature Raman spectra fitted by Gaussian Lorentz of $x = 1/3$ and 2/3 ceramics; (b) $Q \times f$ and FWHM.

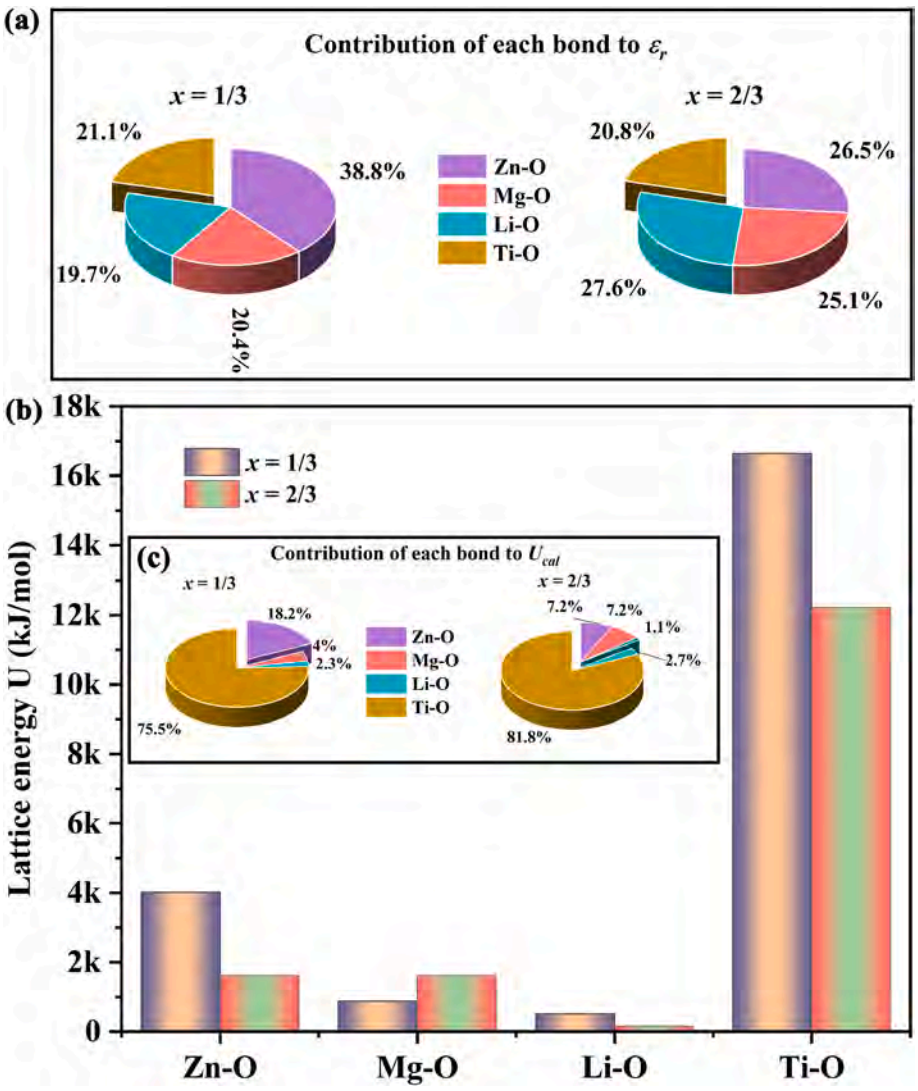

Fig. 7. (a) the contribution of each bond to ε_r; (b) average U_b^μ of the Ti–O bonds; (c) the contributions of individual bonds to the lattice energy for $x = 1/3$ and 2/3 ceramics.

4. Conclusion

ZTLMTx ($x = 1/3$ and 2/3) ceramics were successfully prepared by solid-state reaction route, and the composition-induced change in cation occupancy, crystal structure, and microwave dielectric properties were investigated in detail. The XRD, TEM and Raman spectroscopy analysis showed that the ceramic at $x = 1/3$ exhibited a cubic disordered spinel-structure with a space group of *Fd*-3*m*, whereas the ceramic at $x = 2/3$ showed a cubic ordered spinel-structure with a space group of $P4_332$. Both ceramics were sintered dense at relatively low temperatures (1100 °C for $x = 1/3$ ceramic and 1080 °C for $x = 2/3$ ceramic), significantly lower than the Al-based, Ga-based and Ti-based spinel. The $x = 1/3$ ceramic exhibited the optimal microwave dielectric properties with $\varepsilon_r = 18.27$, high $Q \times f = 91{,}877$ GHz and $\tau_f = -42.3$ ppm/°C. And the ceramic at $x = 2/3$ had a closer to zero τ_f value of −21.05 ppm/°C, along with a larger ε_r of 22.96 and lower $Q \times f$ value of 75,186 GHz. The large relative deviation values (18.3 % and 57 %) between the experimental ε_r and theoretical ε_{th} were observed for $x = 1/3$ and 2/3 ceramics, respectively, due to the underestimation of the ionic polarizability of Ti^{4+}.The specific ordered structures, the wider FWHM of A_{1g}, and lower U_b^μ of $x = 2/3$ ceramic resulted in a lower $Q \times f$ of $x = 2/3$ ceramic than that of $x = 1/3$ ceramic. The higher bond energy of $x = 2/3$ ceramic corresponds to a smaller $|\tau_f|$ than that of $x = 1/3$ ceramic.

Declaration of competing interest

The authors declare that they have no known competing financial interests or personal relationships that could have appeared to influence the work reported in this paper.

Acknowledgments

The authors acknowledge the financial support from the National Natural Science Foundation of China (Nos. 52362017) and Natural Science Foundation of Guangxi Zhuang Autonomous Region (Nos. 2022GXNSFBA035602), and Guangxi Ba Gui Scholars Special Funding.

Appendix A. Supplementary data

Supplementary data to this article can be found online at https://doi.org/10.1016/j.ceramint.2024.01.262.

References

[1] R. Freer, F. Azough, Microstructural engineering of microwave dielectric ceramics, J. Eur. Ceram. Soc. 28 (2008) 1433–1441.
[2] I.M. Reaney, I. David, Microwave dielectric ceramics for resonators and filters in mobile phone networks, J. Am. Ceram. Soc. 89 (2006) 2063–2072.

[3] M.D. Hill, D.B. Cruickshank, I.A. MacFarlane, Perspective on ceramic materials for 5G wireless communication systems, Appl. Phys. Lett. 118 (2021) 120501.

[4] M.T. Sebastian, R. Ubic, H. Jantunen, Low-loss dielectric ceramic materials and their properties, Int. Mater. Rev. 60 (2015) 392–412.

[5] L.Z. Ni, L.X. Li, M.K. Du, Y. Zhan, Wide temperature stable $Ba(Mg_xTa_{2/3})O_3$ microwave dielectric ceramics with ultra-high-Q applied for 5G dielectric filter, Ceram. Int. 47 (2021) 1034–1039.

[6] L.X. Li, Y.T. Li, J.L. Qiao, M.K. Du, Developing high-$Q \times f$ value $MgNb_{2-x}Ta_xO_6$ ($0 \leq x \leq 0.8$) columbite ceramics and clarifying the impact mechanism of dielectric loss: crystal structure, Raman vibrations, microstructure, lattice defects, chemical bond characteristics, structural parameters, and microwave dielectric properties in-depth studies, J. Mater. Sci. Technol. 146 (2023) 186–199.

[7] H.H. Guo, D. Zhou, C. Du, P.-J. Wang, W.-F. Liu, L.X. Pang, Q.P. Wang, J.Z. Su, C. Singh, S. Trukhanov, Temperature stable $Li_2Ti_{0.75}(Mg_{1/3}Nb_{2/3})_{0.25}O_3$-based microwave dielectric ceramics with low sintering temperature and ultra-low dielectric loss for dielectric resonator antenna applications, J. Mater. Chem. C 8 (2020) 4690–4700.

[8] X. Zhang, B. Tang, Z. Fang, H. Yang, Z. Xiong, L. Xue, S. Zhang, Structural evolution and microwave dielectric properties of a novel $Li_3Mg_{2-x/3}Nb_{1-2x/3}Ti_xO_6$ system with a rock salt structure, Inorg. Chem. Front. 5 (2018) 3113–3125.

[9] W. Lei, W.Z. Lu, J.H. Zhu, X.H. Wang, Microwave dielectric properties of $ZnAl_2O_4$–TiO_2 spinel-based composites, Mater. Lett. 61 (2007) 4066–4069.

[10] K.P. Surendran, P.V. Bijumon, P. Mohanan, M.T. Sebastian, (1-x)$MgAl_2O_4$-$xTiO_2$ dielectrics for microwave and millimeter wave applications, Appl. Phys. Mater. Sci. Process 81 (2005) 823–826.

[11] X.C. Lu, Z.H. Du, B. Quan, W.J. Bian, H.K. Zhu, Q.T. Zhang, Structural dependence of the microwave dielectric properties of Cr^{3+}-substituted $ZnGa_2O_4$ spinel ceramics: crystal distortion and vibration mode studies, J. Mater. Chem. C 7 (2019) 8261–8268.

[12] A. Kan, T. Moriyama, S. Takahashi, H. Ogawa, Cation distributions and microwave dielectric properties of spinel-structured $MgGa_2O_4$ ceramics, J. Appl. Phys. 52 (2013) 09KH01.

[13] L.Y. Ao, Y. Tang, J. Li, W.S. Fang, L. Duan, C.X. Su, Y.H. Sun, L.J. Liu, L. Fang, Structure characterization and microwave dielectric properties of $LiGa_5O_8$ ceramic with low-ε_r and low loss, J. Eur. Ceram. Soc. 40 (2020) 5498–5503.

[14] H. Li, R. Xiang, X.Q. Chen, H.W. Hua, S.Q. Yu, B. Tang, G.T. Chen, S.R. Zhang, Intrinsic dielectric behavior of Mg_2TiO_4 spinel ceramic, Ceram. Int. 46 (2020) 4235–4239.

[15] X.Z. Yang, Y.M. Lai, Y.M. Zeng, F. Yang, F.Y. Huang, B.Y. Li, F.S. Wang, C.S. Wu, H. Su, Spinel-type solid solution ceramic $MgAl_2O_4$-Mg_2TiO_4 with excellent microwave dielectric properties, J. Alloy Compd. 898 (2022) 162905.

[16] V.S. Hernandez, L.M.T. Martinez, G.C. Mather, A.R. West, Stoichiometry, structures and polymorphism of spinel-like phases, $Li_{1.33x}Zn_{2-2x}Ti_{1+0.67x}O_4$, J. Mater. Chem. 6 (1996) 1533–1536.

[17] H.T. Kim, Y. Kim, Titanium incorporation in Zn_2TiO_4 spinel ceramics, J. Am. Ceram. Soc. 84 (2001) 1081–1086.

[18] A. Belous, O. Ovchar, D. Durilin, M.M. Krzmanc, M. Valant, D. Suvorov, High-Q microwave dielectric materials based on the spinel Mg_2TiO_4, J. Am. Ceram. Soc. 89 (2010) 3441–3445.

[19] S. Buteea, A.R. Kulkarni, O. Prakasha, R.P.R.C. Aiyar, I. Wattamwar, D. Bais, K. Sudheendrand, K.C. James Raju, Significant enhancement in quality factor of Zn_2TiO_4 with Cu-substitution, Mater. Sci. Eng. B 176 (2011) 567–572.

[20] S. Buteea, A.R. Kulkarni, O. Prakasha, R.P.R.C. Aiyar, K. Sudheendrand, K.C. Raju James, R.F. and microwave dielectric properties of $(Zn_{0.95}M_{0.05})_2TiO_4$ ($M = Mn^{2+}$, Co^{2+}, Ni^{2+} or Cu^{2+}) ceramics, Mater. Sci. Eng. B 168 (2010) 151–155.

[21] C.F. Shih, W.M. Li, M.M. Lin, C.Y. Hsiao, K.T. Hung, Low-temperature sintered Zn_2TiO_4:TiO_2 with near-zero temperature coefficient of resonant frequency at microwave frequency, J. Alloy Compd. 485 (2009) 408–412.

[22] J. Zhang, R.Z. Zuo, Effect of ordering on the microwave dielectric properties of spinel-structured $(Zn_{1-x}(Li_{2/3}Ti_{1/3})_x)_2TiO_4$ ceramics, J. Am. Ceram. Soc. 99 (2016) 1–7.

[23] Y. Tang, Q.B. Du, H.C. Xiang, L. Fang, Tuning the order-disorder of $Zn_{2-2x}Li_xGa_{4+x}O_8$ spinel towards high-performance microwave dielectric ceramic, J. Alloy Compd. 927 (2022) 167026.

[24] S. George, M.T. Sebastian, Synthesis and microwave dielectric properties of novel temperature stable high Q, $Li_2ATi_3O_8$ (A = Mg, Zn) ceramics, J. Am. Ceram. Soc. 93 (2010) 2164–2166.

[25] S.K. Singh, S.R. Kiran, V.R.K. Murthy, Raman spectroscopic and microwave dielectric studies on spinel $Li_2Zn_{(1-x)}Ni_xTi_3O_8$, compounds, Mater. Chem. Phys. 141 (2013) 822–827.

[26] H. Kawai, M. Tabuchi, M. Nagata, H. Tukamoto, A.R. West, Crystal chemistry and physical properties of complex lithium spinels $Li_2MM'_3O_8$ (M=Mg, Co, Ni, Zn; M′=Ti, Ge), J. Mater. Chem. 8 (1998) 1273–1280.

[27] S. George, M.T. Sebastian, Low-temperature sintering and microwave dielectric properties of $Li_2ATi_3O_8$ (A=Mg, Zn) ceramics, Int. J. Appl. Ceram. Technol. 8 (2011) 1400–1407.

[28] M.I. Mendelson, Average grain size in polycrystalline ceramics, J. Am. Ceram. Soc. 52 (1969) 443–446.

[29] Q.B. Du, Y. Tang, J. Li, W.S. Fang, A.H. Yang, J.Q. Chen, L. Fang, A low-εr and high-Q microwave dielectric ceramic Li_2SrSiO_4 with abnormally low sintering temperature, J. Eur. Ceram. Soc. 41 (2021) 7678–7682.

[30] J.Q. Chen, W.S. Fang, Y.F. Zhai, F.H. Li, Y. Tang, J. Li, H.H. Guo, L. Fang, Chemical bond characteristics and infrared reflectivity spectrum of a novel microwave dielectric ceramic $CaIn_2O_4$ with near-zero τ_f, J. Eur. Ceram. Soc. 41 (2021) 4473–4477.

[31] D.S. McClure, The distribution of transition metal cations in spinels, J. Phys. Chem. Solids 3 (1957) 311–317.

[32] J.K. Burdett, G.D. Price, S.L. Price, Role of the crystal-field theory in determining the structures of spinels, J. Am. Chem. Soc. 104 (1982) 92–95.

[33] K. Xia, X.G. Zeng, H.F. Zhu, J. Gong, H. Luo, Mg-doped $Li_2ZnTi_3O_8$/C as high-performance anode materials for lithium-ion batteries, Vacuum 207 (2023) 111614.

[34] C. Moelle, H.J. Fecht, Thermodynamic properties and phase stability of nanocrystalline metals and hydrides, Nanostruct. Mater. 3 (1993) 93–99.

[35] R.D. Shannon, Dielectric polarizabilities of ions in oxides and fluorides, J. Appl. Phys. 73 (1993) 348–366.

[36] Y. Tang, S.Y. Shen, J. Li, X.G. Zhao, H.C. Xiang, H.P. Su, D. Zhou, L. Fang, Characterization of structure and chemical bond in high-Q microwave dielectric ceramics $LiM_2GaTi_2O_8$ (M= Mg, Zn), J. Eur. Ceram. Soc. 42 (2022) 4573–4579.

[37] A. Sayyadi-Shahraki, E. Taheri-Nassaj, H. Barzegar-Bafrooei, S.A. Hassanzadeh-Tabrizi, Microwave dielectric properties of $Li_2ZnTi_3O_8$ ceramics prepared by reaction-sintering process, J. Mater. Sci. Mater. Electron. 25 (2014) 1117–1121.

[38] Y.J. Wang, J. Li, W.S. Fang, Y. Tang, Z.Y. Zhang, H.C. Xiang, L. Fang, A Novel Ultra-high Q Microwave Dielectric Ceramic $ZnMgTiO_4$ with Spinel Structure, doi.org/10.1016/j.ceramint.2023.08.218.

[39] X.Q. Chen, H. Li, P.C. Zhang, H.L. Hu, Y. Tao, G.S. Li, $SrZnV_2O_7$: a low-firing microwave dielectric ceramic with high-quality factor, J. Am. Ceram. Soc. 104 (2021), 00-10.

[40] S.J. Penn, N.M. Alford, A. Templeton, X.R. Wang, M.S. Xu, M. Reece, K. Schrape, Effect of porosity and grain size on the microwave dielectric properties of sintered alumina, J. Am. Ceram. Soc. 80 (1997) 1885–1888.

[41] E.S. Kim, B.S. Chun, R. Freer, Effects of packing fraction and bond valence on microwave dielectric properties of $A^{2+}B^{6+}O_4$ (A^{2+}: Ca, Pb, Ba; B^{6+}: Mo, W) ceramics, J. Eur. Ceram. Soc. 30 (2010) 1731–1736.

[42] I.A. Leonidov, O.N. Leonidova, R.F. Samigullina, M.V. Patrakeev, Structural aspects of lithium transfer in solid electrolytes $Li_{2x}Zn_{2-3x}Ti_{1+x}O_4$ ($0.33 \leq x \leq 0.67$), J. Struct. Chem. 45 (2004) 262–269.

[43] H.R. Tian, J.J. Zheng, L.T. Liu, H.T. Wu, H. Kimura, Y.Z. Lu, Z.X. Yue, Structure characteristics and microwave dielectric properties of $Pr_2(Zr_{1-x}Ti_x)_3(MoO_4)_9$ solid solution ceramic with a stable temperature coefficient, J. Mater. Sci. Technol. 116 (2022) 121–129.

[44] P. Zhang, Y.G. Zhao, Effects of structural characteristics on microwave dielectric properties of $Li_2Mg(Ti_{1-x}Mn_x)_3O_8$ ceramics, J. Alloys Compd. 647 (2015) 386–391.

[45] X. Zhou, L.T. Liu, J.J. Sun, N.K. Zhang, H.Z. Sun, H.T. Wu, W.H. Tao, Effects of $(Mg_{1/3}Sb_{2/3})^{4+}$ substitution on the structure and microwave dielectric properties of $Ce_2Zr_3(MoO_4)_9$ ceramics, J. Adv. Ceram. 10 (2021) 778–789.

[46] K. Liu, L. Shi, X.Y. Wang, C. Liu, J. Li, Y.L. Liao, L.C. Jin, D.N. Zhang, H.W. Zhang, Li^+ enrichment to improve the microwave dielectric properties of $Li_2ZnTi_3O_8$ ceramics and the relationship between structure and properties, J. Eur. Ceram. Soc. 43 (2023) 1483–1491.

[47] C. Xing, J.Z. Li, H.L. Chen, H.Y. Qiao, J. Yang, H.L. Dong, H.Q. Sun, J. Wang, X. Q. Yin, Z.M. Qi, F. Shi, Phonon characteristics, crystal structure, and intrinsic properties of a $Y(Mg_{1/2}Sn_{1/2})O_3$ ceramic, RSV Adv 7 (2017) 35305–35310.

[48] J. Bao, Y. Zhang, H. Kimura, H.T. Wu, Z.X. Yue, Crystal structure, chemical bond characteristics, infrared reflection spectrum, and microwave dielectric properties of $Nd_2(Zr_{1-x}Ti_x)_3(MoO_4)_9$ ceramics, J. Adv. Ceram. 12 (2023) 82–92.

[49] H.Y. Yang, S.R. Zhang, H.C. Yang, Y. Yuan, E.Z. Li, Intrinsic dielectric properties of columbite $ZnNb_2O_6$ ceramics studied by P–V–L bond theory and Infrared spectroscopy, J. Am. Ceram. Soc. 102 (2019) 5365–5374.